

AIE Featured Inorganic–Organic Core@Shell Nanoparticles for High-Efficiency siRNA Delivery and Real-Time Monitoring

Xuwen He,^{†,§,∇} Feng Yin,^{†,‡,∇} Dongyuan Wang,[‡] Ling-Hong Xiong,^{†,§,||} Ryan T. K. Kwok,^{†,§} Peng Fei Gao,^{†,§} Zheng Zhao,^{†,§} Jacky W. Y. Lam,^{†,§} Ken-Tye Yong,[†] Zigang Li,^{*,‡,§} and Ben Zhong Tang^{*,†,§,#}

[†]Department of Chemistry, Hong Kong Branch of Chinese National Engineering Research Centre for Tissue Restoration and Reconstruction, Institute for Advanced Study, Division of Life Science, and Department of Chemical and Biological Engineering, The Hong Kong University of Science and Technology, Clear Water Bay, Kowloon, Hong Kong

[‡]State Key Laboratory of Chemical Oncogenomics, Key Laboratory of Chemical Genomics, School of Chemical Biology and Biotechnology, Peking University Shenzhen Graduate School, Shenzhen 518055, China

[§]HKUST-Shenzhen Research Institute, Shenzhen 518057, China

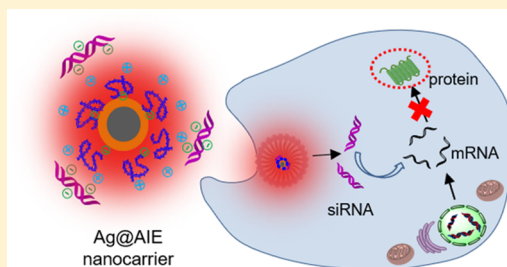
^{||}Shenzhen Center for Disease Control and Prevention, Shenzhen 518055, China

[∇]School of Electrical and Electronic Engineering, Nanyang Technological University, Singapore 639798, Singapore

[#]Center for Aggregation-Induced Emission, SCUT-HKUST Joint Research Laboratory, State Key Laboratory of Luminescent Materials and Devices, South China University of Technology, Guangzhou 510640, China

Supporting Information

ABSTRACT: RNA interference (RNAi) is demonstrated as one of the most powerful technologies for sequence-specific suppression of genes in disease therapeutics. Exploration of novel vehicles for small interfering RNA (siRNA) delivery with high efficiency, low cytotoxicity, and self-monitoring functionality is persistently pursued. Herein, by taking advantage of aggregation-induced emission luminogen (AIEgen), we developed a novel class of Ag@AIE core@shell nanocarriers with regulable and uniform morphology. It presented excellent efficiencies in siRNA delivery, target gene knockdown, and cancer cell inhibition *in vitro*. What's more, an anticancer efficacy up to 75% was achieved in small animal experiments without obvious toxicity. Attributing to the unique AIE properties, real-time intracellular tracking of siRNA delivery and long-term tumor tissue imaging were successfully realized. Compared to the commercial transfection reagents, significant improvements were obtained in biocompatibility, delivery efficiency, and reproducibility, representing a promising future of this nanocarrier in RNAi-related cancer therapeutics.



KEYWORDS: Aggregation-induced emission (AIE), nanocarrier, siRNA, real-time, apoptosis

siRNA with 20–25 base pairs is capable of interfering with specific genes by degrading mRNA (mRNA) and inhibiting the expression of functional protein in gene-disorder-disease therapeutics.^{1–4} In cancer therapy, RNAi functions effectively in knocking down multi-drug-resistance-related protein,⁵ inhibiting the tumorigenesis protein⁶/suppressor mutants⁷ and activating the tumor-associated immune response,⁸ etc. However, due to the small size, siRNA oligos are vulnerable to the RNases in physiological environments. A qualified vehicle for siRNA delivery should significantly enhance its biostability, facilitate the endocytosis, and enrich the siRNA in the target location. To date, numerous vehicles have been developed for siRNA delivery, including lipid/polymer nanoparticles,^{9,10} amphiphilic dendrimers,¹¹ DNA carriers,^{12,13} peptide/protein assemblies,^{14–16} graphene oxide,¹⁷ mesoporous silica,^{18,19} gold nanoparticles/nanorods,^{7,20,21} black phosphorus,²² etc. However, limitations, including cytotoxicity, serious non-specific

absorption, and poor colloidal stability in bio-medium, still accompany these delivery methods. Lack of intrinsic signals is another impediment for real-time monitoring of the intracellular behavior of siRNA. For the high sensitivity and real-time practicability, fluorescence imaging is widely employed to observe the dynamic biochemical process in living systems.^{23,24} Conventional organic fluorophores for cargo siRNA or delivery vehicle labeling, however, usually suffer severe photobleaching that compromise their performance in long-lasting intracellular tracking.²⁵ Although inorganic quantum dots and upconverting nanoparticle-derived^{26–31} nanovehicles possess outstanding brightness and photostability; their heavy metal components-related toxicity still blocks their further clinical translation.^{32–35}

Received: November 20, 2018

Revised: February 26, 2019

Published: March 4, 2019

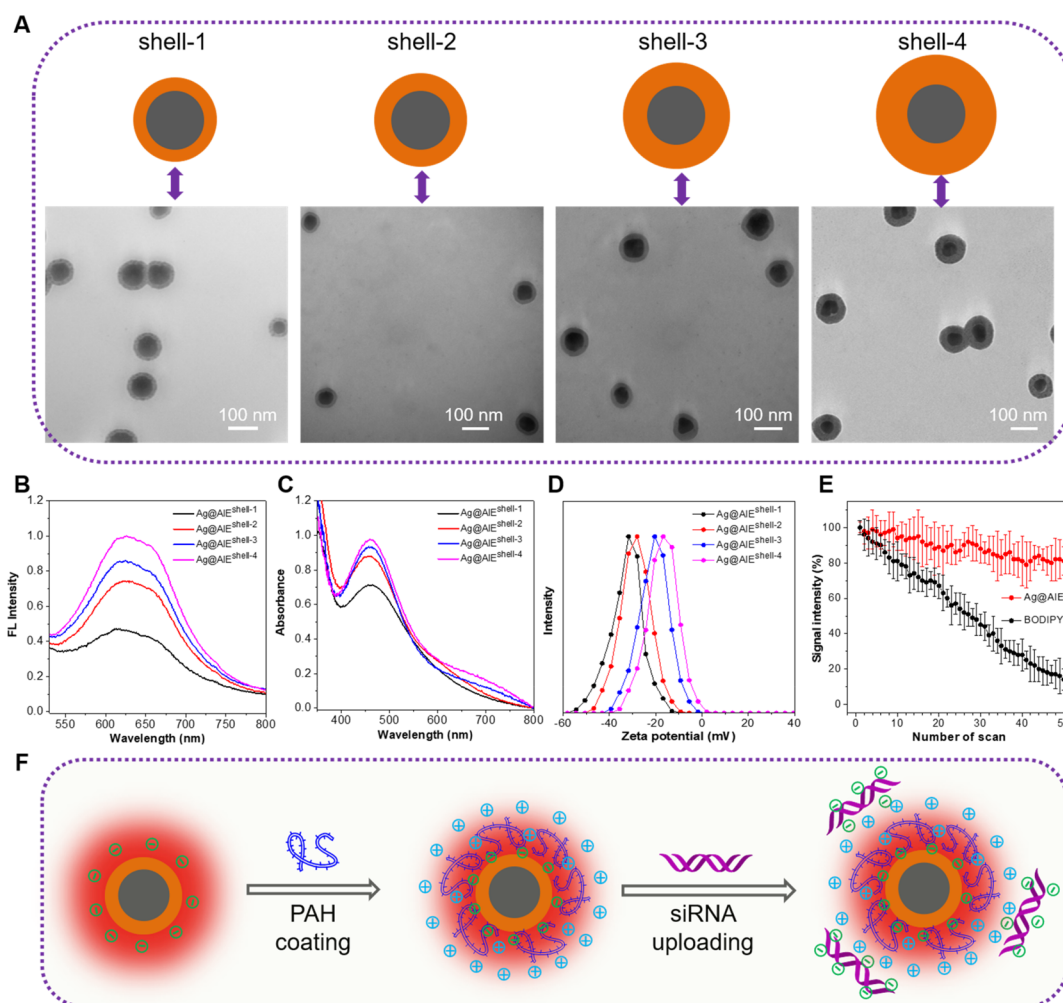


Figure 1. Characterization of Ag@AIE nanoparticles. (A) TEM images, (B) fluorescence spectra, (C) UV–vis spectra, and (D) zeta potential of Ag@AIE nanoparticles (-33.6 , -27.0 , -20.5 , and -16.8 mV for shell-1 to shell-4, respectively). (E) Photostability comparison between Ag@AIE^{shell-2} and BODIPY^{493/503} under confocal laser irradiation. (F) Schematic illustration of the layer-by-layer process for siRNA uploading. The cationic PAH polymer was first wrapped outside the core@shell nanoparticle, followed by uploading of anionic siRNA via electrostatic interaction.

Fortunately, our newly developed AIEgens that emit strongly in the aggregated state through restriction of intramolecular motions behave as a promising alternative. They exhibit wide optical absorptivity, large Stokes shift, robust luminosity, and strong photobleaching resistance, as well as excellent biocompatibility,^{36,37} and have been widely applied in bioanalytes assay,³⁸ organelle/cellular imaging,³⁹ drug delivery tracking,⁴⁰ etc. Nevertheless, the nanoparticles directly formed by AIEgen aggregation through solubility decrease, chemical reaction, or molecular self-assembly are lacking in regularities in their diameter and morphology. The resulting wide-heterogeneity dispersion makes it difficult to precisely control the optical properties, colloidal stabilities, and bioactivities.⁴¹ Although the introduction of surfactants, such as DSPE-PEG/F127,^{42,43} or polymerization⁴⁴ has improved the qualities of nanoparticles in terms of uniformity and homogeneity, the toxic concerns regarding those external surfactants still exist. Attributed to the tunability in diameter and morphology of noble metal nanoparticles,⁴⁵ we recently reported a novel class of Ag@AIE core@shell nanoparticles derived from the simultaneous noble metal ion reduction and AIEgen self-assembly.³⁹ The precisely regulable shell thickness

and unique AIE properties make it a promising candidate for cargo delivery and tracking of intracellular bioactivities.

Herein, excellent performances in siRNA delivery and real-time monitoring were further demonstrated by taking advantage of this tunable core@shell nanovehicle. As shown in Figure 1A, a series of Ag@AIE core@shell nanoparticles with various shell thicknesses were first prepared according to our recent report.³⁹ They were named as Ag@AIE^{shell-1}, Ag@AIE^{shell-2}, Ag@AIE^{shell-3}, and Ag@AIE^{shell-4}, with a shell thickness of 15.6, 21.8, 26.6, and 32.2 nm, respectively (Figure S1). Transmission electron microscope (TEM) images showed their apparent core@shell morphologies as obvious contrast differences emerged between the outer organic and inner inorganic components. With the shell thickness increasing, fluorescence with a maximum at 640 nm of the nanoparticles gradually intensified, indicating the unique AIE property (Figure 1B). In the UV–vis spectra, typical absorption profiles of plasmonic silver nanoparticles appeared with a maximum at 480 nm (Figure 1C). The surface charge evolved from -33.6 to -16.8 mV with the shell thickness increasing from 15.6 to 32.2 nm (Figure 1D). Compared to the traditional fluorophore BODIPY, the AIE nanoparticle showed superior photostability under laser scanning. As shown in Figure 1E, after scanning for

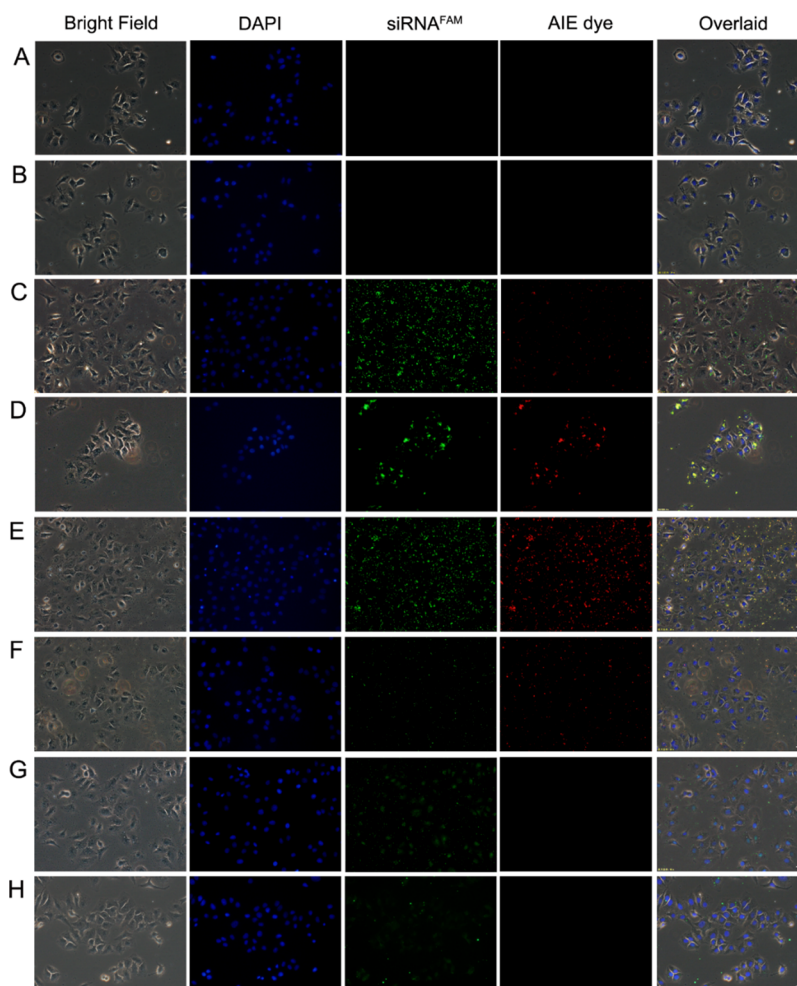


Figure 2. Fluorescent confocal images of intracellular delivery of various formulations into HeLa cells after incubation for 4 h. (A) 1× PBS (blank); (B) free survivin siRNA^{FAM} (negative control); survivin siRNA^{FAM} delivered by PAH-coated (C) Ag@AIE^{shell-1}, (D) Ag@AIE^{shell-2}, (E) Ag@AIE^{shell-3}, and (F) Ag@AIE^{shell-4}; (G) lipofectamine/survivin siRNA^{FAM}, and (H) oligofectamine/survivin siRNA^{FAM} (positive controls). The cell nuclei were stained with DAPI (blue), and signals from FAM and Ag@AIE were green and red, respectively (all of the images were acquired under a 40× objective).

50 times, the Ag@AIE^{shell-2} nanoparticles maintained more than 80% intensity, whereas the BODIPY lost nearly 85% intensity. Excellent photostability was also demonstrated under continuous laser irradiation for Ag@AIE^{shell-2} nanoparticles (Figure S2). These outstanding optical properties indicated their suitability in the long term monitoring of siRNA delivery.

As a proof of concept, survivin siRNA was chosen to test the delivery capability of this core@shell nanocarrier. Survivin protein is expressed highly in most human tumors and functions to inhibit caspase activation, thereby leading to negative regulation of apoptosis.⁴⁶ Previous reports showed that the disruption of survivin induction pathways could facilitate cell apoptosis and inhibit tumor growth and was considered as a good target for RNAi therapy.^{47,48} As illustrated in Figure 1F, through layer-by-layer coating, PAH polymers with positive charge were first shelled around the negative-charged core@shell nanoparticle. The resulting positive-charged Ag@AIE/PAH nanocarrier was then ready for uploading of negative-charged double-strand siRNA. In gel retardation assay, samples with various weight ratios of core/shell nanocarrier to siRNA were uploaded to the wells of agarose gel. Under an electric field, the free siRNA could run quickly in the gel, while the siRNA that attached on the core/

shell nanoparticles could not permeate into the gel due to the large size of the nanocarrier. As a result, when siRNA was completely uploaded by the nanoparticle, the fluorescence signal emitted from the free siRNA would disappear. Therefore, the optimal weight ratios of nanocarrier to siRNA were determined to be 30:1, 20:1, 30:1, and 40:1 for shell-1 to shell-4 nanocarriers, respectively (Figure S3), and the siRNA loading efficiencies were calculated to be 1.776×10^{-14} , 2.809×10^{-14} , 2.026×10^{-14} , and 1.770×10^{-14} mg siRNA per particle for shell-1 to shell-4 nanocarriers, respectively (Table S1). The increase of DLS diameters from 84 to 116 nm, and further to 144 nm, and the alternative changes in zeta potential from -27.0 to $+34.7$ mV, and finally to -41.8 mV, after PAH shelling and siRNA uploading, respectively, verified the successful uploading of survivin siRNA (Figure S4). The Ag@AIE/PAH nanocarrier well protected the siRNAs from the nuclease degradation during 4 h exposure to 10 U/L DNase I (Figure S5), suggesting the great potential of the uploaded siRNA to perform an interference function in cytoplasm. Compared with the delivery agents that condensed or trapped siRNA in their inner space, this core@shell nanocarrier could further promote the intracellular dissociation and release of siRNA for its surface binding mode.

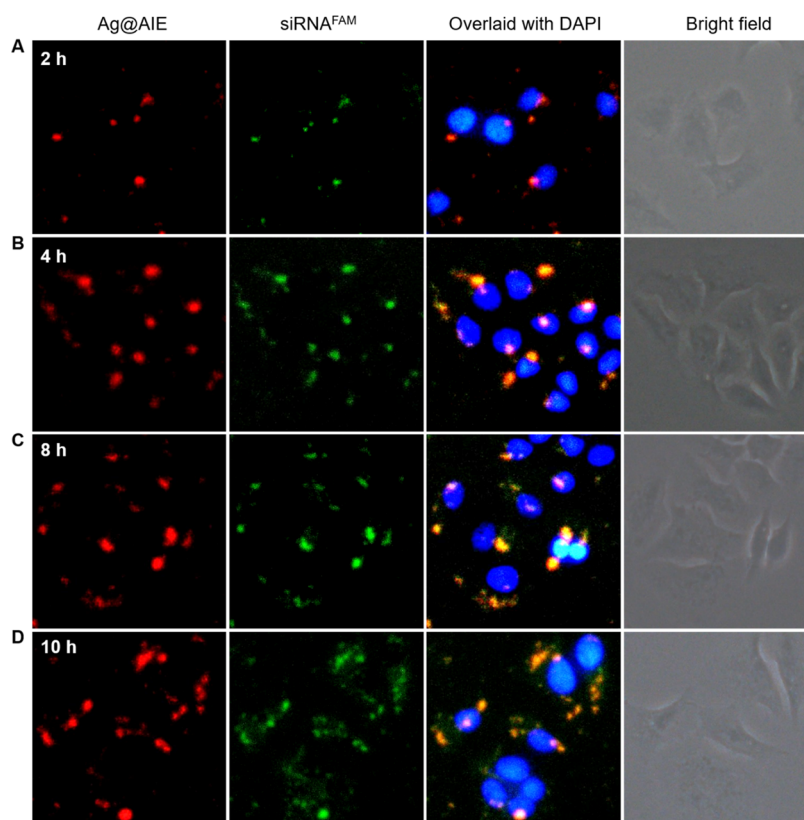


Figure 3. Real-time monitoring of siRNA delivery in HeLa cells at (A) 2 h, (B) 4 h, (C) 8 h, and (D) 10 h time points. The signals from FAM, Ag@AIE, and DAPI (for nuclei staining) were green, red, and blue, respectively (FAM: excited = 488 nm, collected = 500–540 nm; Ag@AIE: excited = 405 nm, collected = 600–700 nm; DAPI: excited = 405 nm, collected = 420–480 nm; and images were captured under a 63 \times oil objective).

The cellular uptake and intracellular distribution of survivin siRNA were next monitored through fluorescence microscopy (Figure 2). siRNA molecules alone were incapable of penetrating the cell membrane. Compared to its counterparts, the Ag@AIE^{shell-2} nanocarrier showed the strongest red (Ag@AIE nanocarrier) and green fluorescence (siRNA^{FAM}), indicating its highest efficiency in siRNA transfection. More interesting, the fluorescence signals from commercial reagents (both Lipofectamine-2000 and Oligofectamine) were much weaker than from Ag@AIE^{shell-2}/PAH/siRNA, suggesting a much higher endocytosis efficiency from this core@shell nanovehicle. The colloidal stability of nanoparticles was proposed to exert a significant influence in the transfection efficiency. The Ag@AIE^{shell-2} nanocarrier presented little fluctuation in fluorescence and in its absorption profile during 15 d of storage, and its diameter changed little compared to the fresh prepared counterpart (Figures S6 and S7), whereas the shell-3 and shell-4 nanocarriers seriously agglomerated with hydrodynamic size increasing to \sim 900 and \sim 1700 nm, respectively (Figure S8). TEM imaging also verified these agglomerations (Figure S9). Although the Ag@AIE^{shell-1} nanocarrier displayed negligible change in hydrodynamic size, it was inclined to cross-link when confronting the positive-charged PAH polymer due to the large electrical difference between them. Consequently, the stability of Ag@AIE^{shell-2} nanocarrier mainly resulted from its suitable zeta potential value, and it was chosen as the survivin siRNA delivery vehicle in the following studies. Flow cytometry analysis was performed to further quantitate the siRNA delivery efficiency (Figure S10). HeLa cells treated with

Ag@AIE^{shell-2}/PAH/survivin siRNA exhibited strong green and red fluorescence. The corresponding transfection efficiencies were calculated to be 96.1% and 94.9%, respectively, which were much higher than those for Oligofectamine/siRNA formulations. The difference between flow cytometry analysis and fluorescence microscopic imaging may be a result from the agglomeration or cross-linking of shell-1, -3, and -4 nanoparticles on cell membrane without internalization.

Contributing to the intrinsic fluorescence of AIEgen, the intracellular behaviors of siRNA were successfully monitored in real time. As shown in Figure 3, the transportation across the plasma membrane of the siRNAs was verified by the intracellular green fluorescence post 2 h transfection. The perfect overlap of FAM and Ag@AIE channels (orange merged by green and red) indicated the tight binding between siRNA and the nanocarrier. That would protect the siRNA from the enzymatic degradation in the early endocytosis stage. The siRNA molecules started to separate from the Ag@AIE vehicle until 8 h (separated green signal in the overlaid channel) and became evenly distributed in the cytoplasm after 10 h incubation with gradual decrease in colocalization efficiency (Figure S11), confirming their gradual release from the surface of Ag@AIE nanocarrier for subsequent RNA interference in cancer cells. The endosome escape, dissociation from carrier, and coupling with cellular machines (the RNA-induced silencing complex) determine the intracellular siRNA delivery efficiency. Previous reports showed that the amino group could buffer the interior acidic environment of endosomes to some extent, thereby inducing their osmotic swelling and rupture of the endosomal membrane. The so-called “proton sponge”

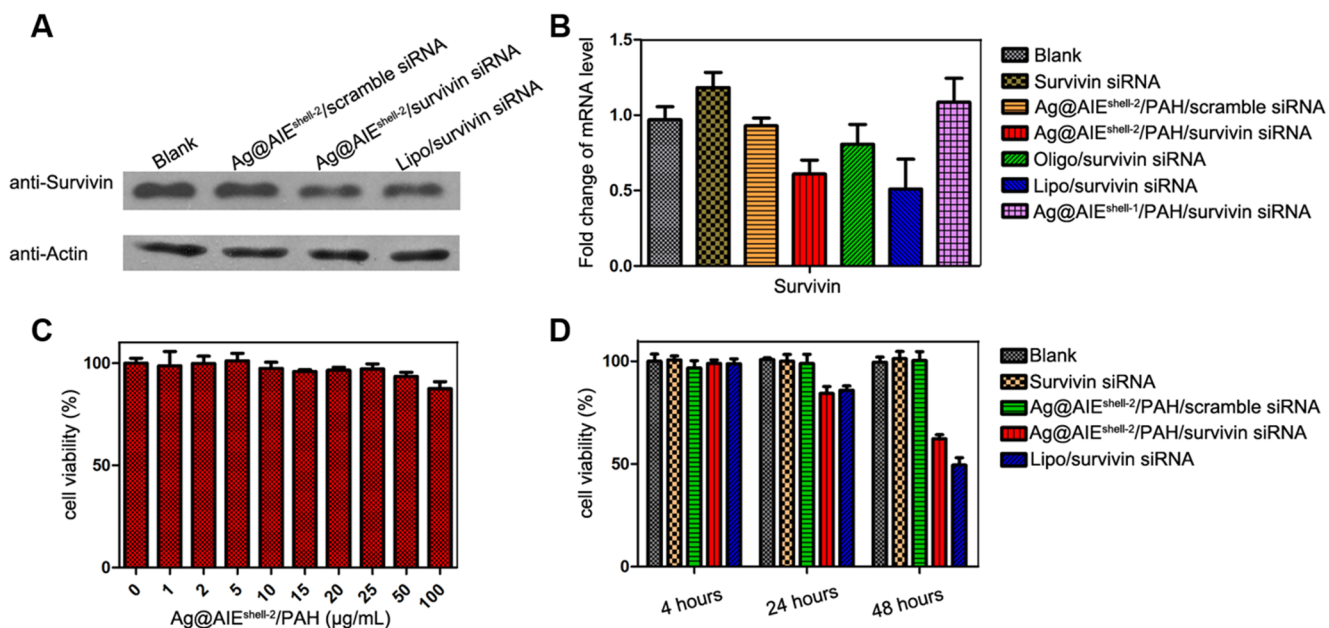


Figure 4. Evaluations of gene expression level and cell viability. (A) Relative protein level of survivin detected by Western blotting. Actin was used as the protein loading control. (B) Fold change of the mRNA level of survivin was detected by RT-PCR after 48 h. The knockdown efficiency was equal to the fold change subtracted by 1.0. (C) The toxicity test of Ag@AIE/PAH to HeLa cells after 48 h co-incubation. (D) Cell viability test for various siRNA formulations with time elapsing. Data are presented as means \pm SEM of triplicate experiments.

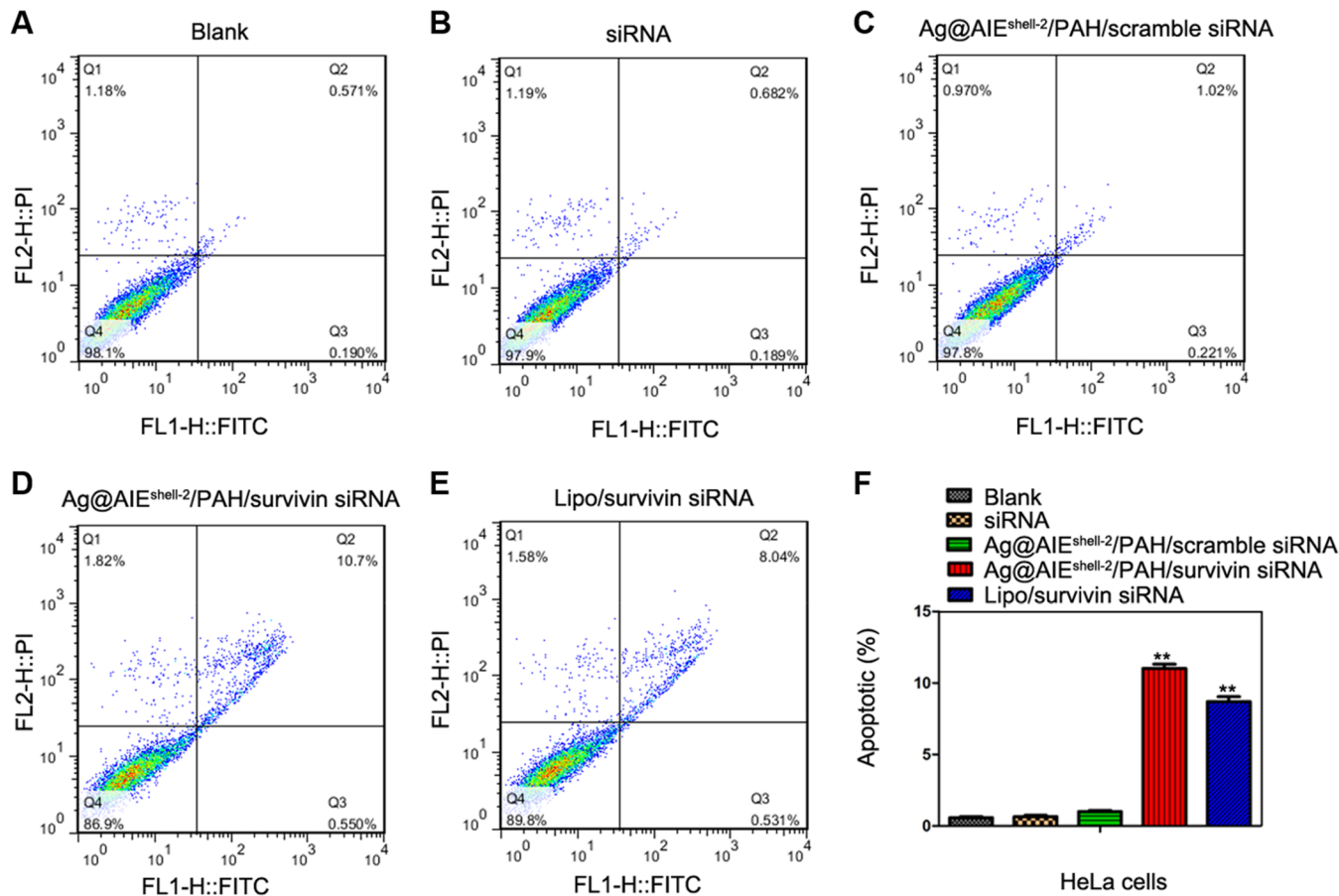


Figure 5. FITC-Annexin V and propidium iodide (PI) stained cell death assay via flow cytometry. HeLa cells were treated with different formulations for 48 h. (A–E) The number of apoptotic cells stained with Annexin V/PI measured by flow cytometry with various interferences. (F) Late apoptotic cell counts in the upper right quadrant (Q2) and lower right quadrant (Q3) for different treatment groups. Data are presented as means \pm SEM of triplicate experiments (* P < 0.05 and ** P < 0.01 vs PBS blank).

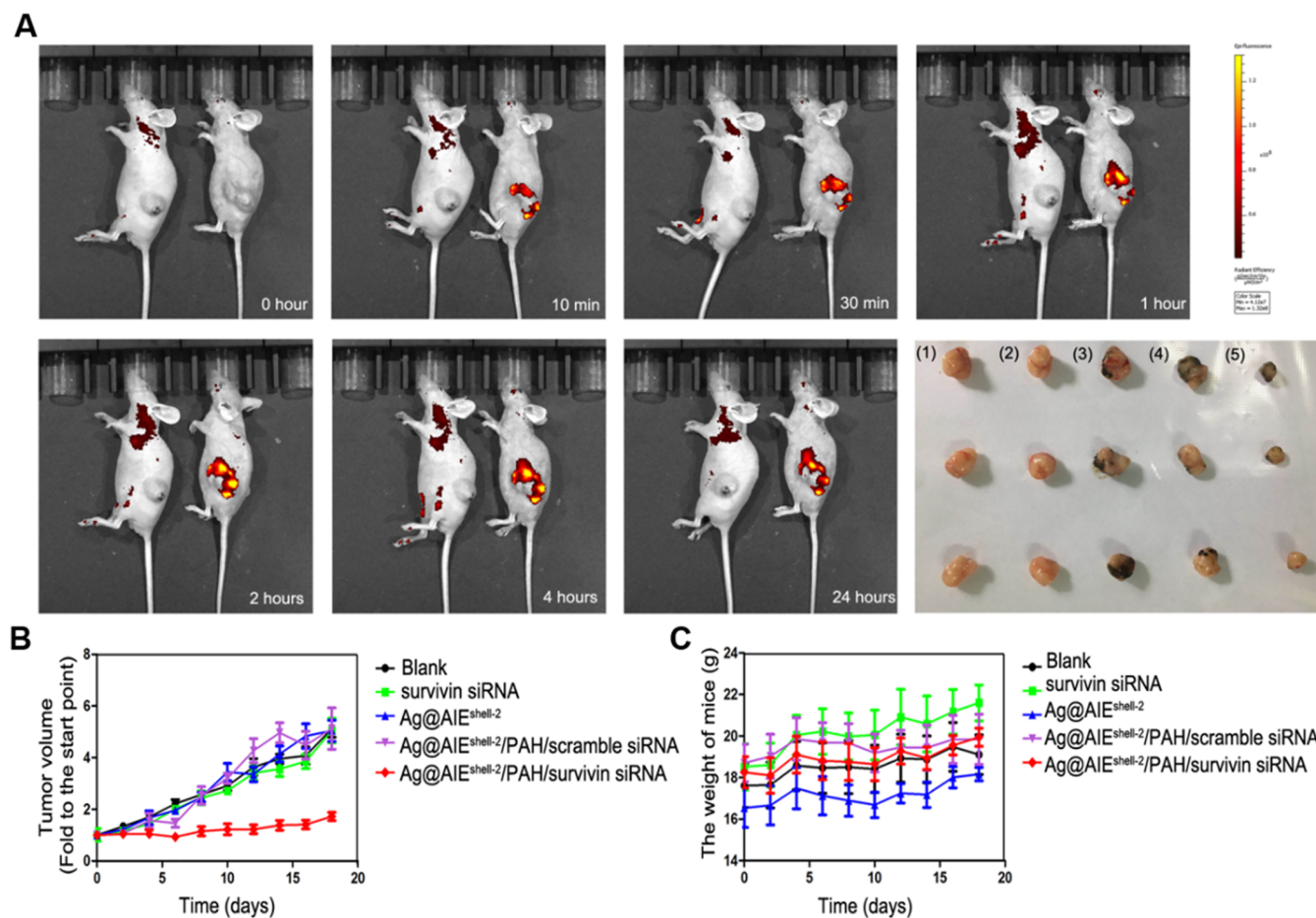


Figure 6. In vivo fluorescence imaging and RNA interference therapy practice. (A) Fluorescence imaging of tumor tissues in HeLa tumor-bearing mice at different time points after intratumoral injection of PBS or Ag@AIE^{shell-2}/PAH/survivin siRNA and the representative images of tumor tissues treated with (1) PBS blank, (2) free survivin siRNA, (3) nude Ag@AIE nanocarrier, (4) Ag@AIE^{shell-2}/PAH/scramble siRNA, and (5) Ag@AIE^{shell-2}/PAH/survivin siRNA. (B) The volume growth curves of tumors at different time points post-treatment in each group. (C) Body weight measurements of the mice in each group. The data represent the means \pm SEM.

effect contributed to the release of the uploaded siRNA and promoting the siRNA delivery efficiency.^{49–51} Herein, the moderate surface charge and excellent colloidal stability of Ag@AIE^{shell-2} nanocarrier as well as the amine groups of the PAH-coating layer could facilitate the intracellular release and target recognition/interference of the uploaded siRNA.

Given the significant role of survivin in cancer apoptosis, our siRNA nanocarrier was next tested in gene knockdown regulation. The amount of survivin gene knockdown was quantitated in mRNA and protein level through reverse transcription polymerase chain reaction (RT-PCR) and Western blotting (WB) assays, respectively. As shown in Figure 4A and B, similar to the PBS group, HeLa cells treated with nude nanocarrier and Ag@AIE/PAH/scramble siRNA formulation both exhibited negligible changes in the target mRNA or protein level. In contrast, Ag@AIE^{shell-2}/PAH/survivin siRNA treatment showed a remarkably inhibitory effect to the expression of survivin gene with a knockdown efficiency up to 38%. It even surpassed the oligofectamine/survivin siRNA with a knockdown efficiency of 19%. Although the lipofectamine/survivin siRNA presented a little bit higher efficiency of 49%; the much broader error bar indicated its poor reproducibility. On the other hand, the nude Ag@AIE/PAH nanocarrier exhibited excellent biocompatibility. As shown in Figure 4C, HeLa cells even remained with 90%

viability after treatment with 100 μ g/mL Ag@AIE/PAH nanocarrier for 48 h. The capability of siRNA uploaded nanocarrier in inhibiting cancer cell growth was next tested (Figure 4D). As expected, there was negligible inhibition in cancer cell growth after incubation with nude nanocarrier or Ag@AIE/PAH/scramble siRNA formulation. In contrast, obvious inhibition with an efficiency up to 40% could be observed for Ag@AIE/PAH/survivin siRNA. Further, flow cytometric assay in Figure 5 showed that the apoptotic efficiency was up to 10.7% for Ag@AIE/PAH/survivin siRNA, which was significantly higher than blank (0.57%), free siRNA (0.66%), and scramble siRNA-loaded nanocarrier (0.94%). The even better performance compared to lipofectamine (10.7% vs 8.04%) in triggering cell apoptosis indicated its superiority in RNAi therapeutics.

Inspired by these outstanding performances in cellular experiments, we further applied this core@shell nanocarrier for RNAi in tumor-bearing mice. As shown in Figure 6A, after intratumoral injection of Ag@AIE/PAH/survivin siRNA (640 μ g with 32 μ g siRNA), intense fluorescence signals could be continuously observable at the tumor site even after 24 h post-injection. The mice were then sacrificed at 24 h and the ex vivo fluorescence images of isolated tissues showed that the core@shell nanocarrier effectively accumulated in the tumor tissue yielding robust emission intensity. Subsequently, the ther-

apeutic effect of Ag@AIE/PAH/survivin siRNA formulation for in vivo tumor inhibition was examined. The mice were treated with Ag@AIE/PAH/survivin siRNA (320 μg with 16 μg siRNA) every 2 days starting on day-0 and lasting for 18 days. As shown in Figure 6B, compared to the PBS group, free survivin siRNA, nude Ag@AIE carrier, or Ag@AIE/PAH/scramble siRNA formulation, mice injected with Ag@AIE/PAH/survivin siRNA formulation showed the strongest inhibitory effect in tumor growth after 18 d of treatment. Noteworthy, similar to the PBS group, negligible body weight losses were observed in the mice treated with the core@shell nanocarrier and its siRNA formulation (Figure 6C). The histological analyses of major organs (heart, liver, spleen, lung, kidneys, brain, tumor) further demonstrated the excellent biocompatibility of this core@shell nanof ormulation in vivo, as obvious lesions only happened in the tumor tissues (Figure S12). The remarkable down-regulations in survivin protein level could also be found in the immunohistologic staining of tumor tissues in the Ag@AIE^{shell-2}/PAH/survivin siRNA-treated group, confirming the excellent survivin siRNA delivery efficiency by the core@shell nanocarrier (Figure S13).

In summary, a novel class of AIE-featured core@shell nanovehicles for siRNA delivery and monitoring was successfully demonstrated. The main problem that was solved by using this AIE nanoparticle was to facilitate the delivery efficiency of siRNA and provide a superior stable labeling method for real-time monitoring of its intracellular behaviors. The thickness of the AIE shell was optimized for high-efficiency siRNA delivery in vitro and in vivo, with excellent performances in targeting mRNA interference and tumor growth inhibition. The cellular endocytosis, endosomal escape of siRNA, and in vivo tumor tissue were real-time visualized by harnessing its unique AIE fluorescence signal. Outperforming to the lipo-based commercial transfection agents, the higher efficiency and reproducibility in target regulation as well as lower cytotoxicity of this nanovehicle represent its prospective future in RNAi-based therapeutic applications.

■ ASSOCIATED CONTENT

Supporting Information

The Supporting Information is available free of charge on the ACS Publications website at DOI: 10.1021/acs.nanolett.8b04677.

Materials, experimental sections, and Figures S1–S13 (PDF)

■ AUTHOR INFORMATION

Corresponding Authors

*E-mail: tangbenz@ust.hk.

*E-mail: lizg@pkusz.edu.cn.

ORCID

Xuwen He: 0000-0002-8414-5164

Ryan T. K. Kwok: 0000-0002-6866-3877

Ken-Tye Yong: 0000-0001-7936-2941

Zigang Li: 0000-0002-3630-8520

Ben Zhong Tang: 0000-0002-0293-964X

Author Contributions

[†]These authors contributed equally.

Notes

The authors declare no competing financial interest.

■ ACKNOWLEDGMENTS

The authors acknowledge funding to B.Z.T. from the Innovation and Technology Commission (ITC-CNRC14SC01 and ITS/254117), the National Science Foundation of China (NSFC 21788102), and the Research Grants Council of Hong Kong (16305015, N_HKUST604/14, A-HKUST605/16, and C6009-17G). B.Z.T. is also grateful for the support from the Science and Technology Plan of Shenzhen (JCYJ20160229205601482). The authors also acknowledge funding to Z.L. (NSFC 1778009), F.Y. (NSFC 81701818), and L.-H.X. (NSFC 21705111).

■ REFERENCES

- (1) Agrawal, N.; Dasaradhi, P. V. N.; Mohammed, A.; Malhotra, P.; Bhatnagar, R. K.; Mukherjee, S. K. *Microbiol. Mol. Biol. Rev.* **2003**, *67*, 657–685.
- (2) Elbashir, S. M.; Harborth, J.; Lendeckel, W.; Yalcin, A.; Weber, K.; Tuschl, T. *Nature* **2001**, *411*, 494–498.
- (3) Wittrup, A.; Lieberman, J. *Nat. Rev. Genet.* **2015**, *16*, 543–552.
- (4) Fan, W.; Yung, B.; Huang, P.; Chen, X. *Chem. Rev.* **2017**, *117*, 13566–13638.
- (5) MacDiarmid, J. A.; Amaro-Mugridge, N. B.; Madrid-Weiss, J.; Sedliarou, I.; Wetzel, S.; Kochar, K.; Brahmabhatt, V. N.; Phillips, L.; Pattison, S. T.; Petti, C.; Stillman, B.; Graham, R. M.; Brahmabhatt, H. *Nat. Biotechnol.* **2009**, *27*, 643–651.
- (6) Jensen, S. A.; Day, E. S.; Ko, C. H.; Hurley, L. A.; Luciano, J. P.; Kouri, F. M.; Merkel, T. J.; Luthi, A. J.; Patel, P. C.; Cutler, J. I.; Daniel, W. L.; Scott, A. W.; Rotz, M. W.; Meade, T. J.; Giljohann, D. A.; Mirkin, C. A.; Stegh, A. H. *Sci. Transl. Med.* **2013**, *5*, 209ra152–209ra152.
- (7) Yin, F.; Yang, C.; Wang, Q.; Zeng, S.; Hu, R.; Lin, G.; Tian, J.; Hu, S.; Lan, R. F.; Yoon, H. S.; Lu, F.; Wang, K.; Yong, K.-T. *Theranostics* **2015**, *5*, 818–833.
- (8) Kortylewski, M.; Swiderski, P.; Herrmann, A.; Wang, L.; Kowolik, C.; Kujawski, M.; Lee, H.; Scuto, A.; Liu, Y.; Yang, C.; Deng, J.; Soifer, H. S.; Raubitschek, A.; Forman, S.; Rossi, J. J.; Pardoll, D. M.; Jove, R.; Yu, H. *Nat. Biotechnol.* **2009**, *27*, 925–932.
- (9) Gilleron, J.; Querbes, W.; Zeigerer, A.; Borodovsky, A.; Marsico, G.; Schubert, U.; Manygoats, K.; Seifert, S.; Andree, C.; Stöter, M.; Epstein-Barash, H.; Zhang, L.; Kotliansky, V.; Fitzgerald, K.; Fava, E.; Bickle, M.; Kalaidzidis, Y.; Akinc, A.; Maier, M.; Zerial, M. *Nat. Biotechnol.* **2013**, *31*, 638–646.
- (10) Xu, X.; Wu, J.; Liu, Y.; Saw, P. E.; Tao, W.; Yu, M.; Zope, H.; Si, M.; Victorious, A.; Rasmussen, J.; Ayyash, D.; Farokhzad, O. C.; Shi, J. *ACS Nano* **2017**, *11*, 2618–2627.
- (11) Liu, X.; Zhou, J.; Yu, T.; Chen, C.; Cheng, Q.; Sengupta, K.; Huang, Y.; Li, H.; Liu, C.; Wang, Y.; Posocco, P.; Wang, M.; Cui, Q.; Giorgio, S.; Fermeglia, M.; Qu, F.; Prisel, S.; Shi, Y.; Liang, Z.; Rocchi, P.; Rossi, J. J.; Peng, L. *Angew. Chem., Int. Ed.* **2014**, *53*, 11822–11827.
- (12) Bujold, K. E.; Hsu, J. C. C.; Sleiman, H. F. *J. Am. Chem. Soc.* **2016**, *138*, 14030–14038.
- (13) Rahman, M. A.; Wang, P.; Zhao, Z.; Wang, D.; Nannapaneni, S.; Zhang, C.; Chen, Z.; Griffith, C. C.; Hurwitz, S. J.; Chen, Z. G.; Ke, Y.; Shin, D. M. *Angew. Chem., Int. Ed.* **2017**, *56*, 16023–16027.
- (14) Tai, W.; Gao, X. *Adv. Drug Delivery Rev.* **2017**, *110–111*, 157–168.
- (15) Tai, W.; Li, J.; Corey, E.; Gao, X. *Nat. Biomed. Eng.* **2018**, *2*, 326–337.
- (16) Li, W.; Wang, D.; Shi, X.; Li, J.; Ma, Y.; Wang, Y.; Li, T.; Zhang, J.; Zhao, R.; Yu, Z.; Yin, F.; Li, Z. *Mater. Horiz.* **2018**, *5*, 745–752.
- (17) Yin, F.; Hu, K.; Chen, Y.; Yu, M.; Wang, D.; Wang, Q.; Yong, K.-T.; Lu, F.; Liang, Y.; Li, Z. *Theranostics* **2017**, *7*, 1133–1148.
- (18) Yin, F.; Zhang, B.; Zeng, S.; Lin, G.; Tian, J.; Yang, C.; Wang, K.; Xu, G.; Yong, K.-T. *J. Mater. Chem. B* **2015**, *3*, 6081–6093.
- (19) Feng, Y.; Panwar, N.; Tng, D. J. H.; Tjin, S. C.; Wang, K.; Yong, K.-T. *Coord. Chem. Rev.* **2016**, *319*, 86–109.

- (20) Nemati, H.; Ghahramani, M.-H.; Faridi-Majidi, R.; Izadi, B.; Bahrami, G.; Madani, S.-H.; Tavoosidana, G. *J. Controlled Release* **2017**, *268*, 259–268.
- (21) Rosi, N. L.; Giljohann, D. A.; Thaxton, C. S.; Lytton-Jean, A. K. R.; Han, M. S.; Mirkin, C. A. *Science* **2006**, *312*, 1027–1030.
- (22) Yin, F.; Hu, K.; Chen, S.; Wang, D.; Zhang, J.; Xie, M.; Yang, D.; Qiu, M.; Zhang, H.; Li, Z.-G. *J. Mater. Chem. B* **2017**, *5*, 5433–5440.
- (23) Baker, M. *Nature* **2010**, *463*, 977–980.
- (24) Kobayashi, H.; Ogawa, M.; Alford, R.; Choyke, P. L.; Urano, Y. *Chem. Rev.* **2010**, *110*, 2620–2640.
- (25) Luo, J.; Xie, Z.; Lam, J. W.; Cheng, L.; Chen, H.; Qiu, C.; Kwok, H. S.; Zhan, X.; Liu, Y.; Zhu, D.; Tang, B. Z. *Chem. Commun.* **2001**, 1740–1741.
- (26) Wang, Y.; Wu, B.; Yang, C.; Liu, M.; Sum, T. C.; Yong, K.-T. *Small* **2016**, *12*, 534–546.
- (27) Yezhelyev, M. V.; Qi, L.; O'Regan, R. M.; Nie, S.; Gao, X. *J. Am. Chem. Soc.* **2008**, *130*, 9006–9012.
- (28) Lin, M.; Gao, Y.; Diefenbach, T. J.; Shen, J. K.; Hornicek, F. J.; Park, Y. I.; Xu, F.; Lu, T. J.; Amiji, M.; Duan, Z. *ACS Appl. Mater. Interfaces* **2017**, *9*, 7941–7949.
- (29) Wei, W.; He, X.; Ma, N. *Angew. Chem., Int. Ed.* **2014**, *53*, 5573–5577.
- (30) Wu, D.; Song, G.; Li, Z.; Zhang, T.; Wei, W.; Chen, M.; He, X.; Ma, N. *Chem. Sci.* **2015**, *6*, 3839–3844.
- (31) Gao, L.; Ma, N. *ACS Nano* **2012**, *6*, 689–695.
- (32) Xiong, L.-H.; Cui, R.; Zhang, Z.-L.; Yu, X.; Xie, Z.; Shi, Y.-B.; Pang, D.-W. *ACS Nano* **2014**, *8*, 5116–5124.
- (33) He, X.; Ma, N. *Colloids Surf., B* **2014**, *124*, 118–31.
- (34) He, X.; Zeng, T.; Li, Z.; Wang, G.; Ma, N. *Angew. Chem., Int. Ed.* **2016**, *55*, 3073–3076.
- (35) Yong, K.-T.; Law, W.-C.; Hu, R.; Ye, L.; Liu, L.; Swihart, M. T.; Prasad, P. N. *Chem. Soc. Rev.* **2013**, *42*, 1236–1250.
- (36) Mei, J.; Leung, N. L.; Kwok, R. T.; Lam, J. W.; Tang, B. Z. *Chem. Rev.* **2015**, *115*, 11718–940.
- (37) Mei, J.; Hong, Y.; Lam, J. W. Y.; Qin, A.; Tang, Y.; Tang, B. Z. *Adv. Mater.* **2014**, *26*, 5429–5479.
- (38) Xiong, L.-H.; He, X.; Zhao, Z.; Kwok, R. T. K.; Xiong, Y.; Gao, P. F.; Yang, F.; Huang, Y.; Sung, H. H. Y.; Williams, I. D.; Lam, J. W. Y.; Cheng, J.; Zhang, R.; Tang, B. Z. *ACS Nano* **2018**, *12*, 9549–9559.
- (39) He, X.; Zhao, Z.; Xiong, L.-H.; Gao, P. F.; Peng, C.; Li, R. S.; Xiong, Y.; Li, Z.; Sung, H. H. Y.; Williams, I. D.; Kwok, R. T. K.; Lam, J. W. Y.; Huang, C. Z.; Ma, N.; Tang, B. Z. *J. Am. Chem. Soc.* **2018**, *140*, 6904–6911.
- (40) Yuan, Y.; Liu, B. *Chem. Sci.* **2017**, *8*, 2537–2546.
- (41) Albanese, A.; Tang, P. S.; Chan, W. C. *Annu. Rev. Biomed. Eng.* **2012**, *14*, 1–16.
- (42) Li, M.; Gao, Y.; Yuan, Y.; Wu, Y.; Song, Z.; Tang, B. Z.; Liu, B.; Zheng, Q. C. *ACS Nano* **2017**, *11*, 3922–3932.
- (43) Mao, D.; Wu, W.; Ji, S.; Chen, C.; Hu, F.; Kong, D.; Ding, D.; Liu, B. *Chem.* **2017**, *3*, 991–1007.
- (44) Yuan, Y.; Zhang, C. J.; Liu, B. *Angew. Chem., Int. Ed.* **2015**, *54*, 11419–11423.
- (45) Xia, Y.; Xiong, Y.; Lim, B.; Skrabalak, S. E. *Angew. Chem., Int. Ed.* **2009**, *48*, 60–103.
- (46) Tamm, I.; Wang, Y.; Sausville, E.; Scudiero, D. A.; Vigna, N.; Oltersdorf, T.; Reed, J. C. *Cancer Res.* **1998**, *58*, 5315–5320.
- (47) Mita, A. C.; Mita, M. M.; Nawrocki, S. T.; Giles, F. J. *Clin. Cancer Res.* **2008**, *14*, 5000–5005.
- (48) Zaffaroni, N.; Pannati, M.; Diadone, M. G. *J. Cell. Mol. Med.* **2005**, *9*, 360–372.
- (49) Neu, M.; Fischer, D.; Kissel, T. J. *Gene Med.* **2005**, *7*, 992–1009.
- (50) Duan, H.; Nie, S. *J. Am. Chem. Soc.* **2007**, *129*, 3333–3338.
- (51) Qi, L.; Gao, X. *ACS Nano* **2008**, *2*, 1403–1410.